Supporting Information

Star-Polymer-DNA Gels
Showing Highly Predictable and Tunable Mechanical Responses

*Masashi Ohira[1], Takuya Katashima[1], Mitsuru Naito[2], Daisuke Aoki[3], Yusuke Yoshikawa[4], Hiroki Iwase[5], Shin-ichi Takata[6], Kanjiro Miyata[7], Ung-il Chung[1], Takamasa Sakai[1], Mitsuhiro Shibayama[5] and Xiang Li[8]**

[1]*Department of Bioengineering, Graduate School of Engineering, The University of Tokyo, 7-3-1 Hongo, Bunkyo-ku, Tokyo, 113-8685, Japan*

[2]*Center for Disease Biology and Integrative Medicine, Graduate School of Medicine, The University of Tokyo, 7-3-1 Hongo, Bunkyo-ku, Tokyo, 113-0033, Japan*

[3]*Department of Chemical Science and Engineering, Tokyo Institute of Technology, 2-12-1 Ookayama, Meguro-ku, 152-8550, Tokyo, Japan*

[4]*Neutron Science Laboratory, Institute for Solid State Physics, The University of Tokyo, 5-1-5 Kashiwanoha, Kashiwa, Chiba 277-8581, Japan*

[5]*Neutron Science and Technology Center, Comprehensive Research Organization for Science and Society (CROSS), 162-1 Shirakata, Tokai, Naka, Ibaraki, 319-1106, Japan*

[6]*Materials and Life Science Division, J-PARC Center, Japan Atomic Energy Agency (JAEA), 2-4 Shirakata, Tokai, Ibaraki 319-1195, Japan*

[7]*Department of Materials Engineering, Graduate School of Engineering, The University of Tokyo, 7-3-1 Hongo, Bunkyo-ku, Tokyo, 113-8656, Japan*

[8]*Faculty of Advanced Life Science, Hokkaido University, Sapporo 001-0021, Japan*

*Correspondence to: Xiang Li, x.li@sci.hokudai.ac.jp

Table of Contents

1 Materials

Oligonucleotides (sense strand: 5'-TCGCAACAATAACTGA-3', antisense strand: 5'-TCAGTTATTGTTGCGA-3') terminated with an amine group at the 5'-position by the 5'-amino modifier C6 were purchased from Integrated DNA Technologies (IDT), USA. These sequences were designed to have no stem-loops and other stable intermediates. 3' end labeled with fluorescein (FAM) and black hole quencher 1 (BHQ1) oligonucleotides of the sense and antisense sequences were purchased from Hokkaido Systems Science. Four-armed polyethylene glycols (PEG) (Mn = 40k) terminated with *N*-hydroxysuccinimide (NHS) ester were purchased from NOF Corp. Sodium hydrogen carbonate, sodium carbonate, triethylamine, acetate acid, dimethyl sulfoxide, and phosphate buffer (pH 7.4, 100 mM) were purchased from FUJIFILM Waco Chemicals. In all experiments, 100 mM phosphate buffer was diluted to 25 mM for use.

2 Methods

2.1 Computational design of oligonucleotides

The oligo DNA was designed with DINAMelt[1] and NUPACK[2] to be an ideal dynamic crosslinker; i.e., the DNA undergoes a simple two-state transition to dissociate from duplex to single strands and vice versa, without forming a nonideal association. In these calculations, the experimental sodium concentration (37.5 mM) was used. This sodium concentration was calculated from the sodium phosphate buffer used in this study (pH 7.4, 25 mM).

2.2 Reversed-phase HPLC (analytical)

Reversed-phase HPLC (RP-HPLC) was performed on a Shimadzu Prominence system with an SPD-M20A photodiode array detector (set to 260 nm) with a 10 mm flow cell. Chromatography was performed using a Jupiter column (250 x 4.6 mm, 5 μm particle size, Phenomenexm) at 40 °C, running a gradient with a flow rate of 1 mL/min from 90% A and 10% B to 30% A and 70% B in 30 min. Solvent A: 100 mM, pH 7 triethylamine/acetic acid aqueous buffer. Solvent B: acetonitrile.

2.3 Size exclusion chromatography (preparative)

Size exclusion chromatography (SEC) was performed using the Shimadzu Prominence system with an SPD-M20A photodiode array detector (set to 260 nm) with a 0.1 mm flow cell and an RID-20A refractive index detector. Two Superdex 200 increase columns (10x300 mm, Cytiva) were used at room temperature with a flow rate of 1 mL/min using triethylamine/acetic acid aqueous buffer (100 mM, pH 7).

2.4 Photography

Photographs of the gel samples were taken using a Nikon D5300. SYBR green I was added to the gel sample as a probe for DNA duplex. The gel sample was filled in an NMR tube and heated by a hair dryer. Fluorescence images were pictured using the camera with a 500 nm long-pass filter, in the presence of the excitation light from a 470 nm LED light source (M470F3, Thorlabs).

2.5 Melting curve analysis

UV absorbance measurements were performed on a UV-VIS spectrometer (V-630, JASCO). A gel sample and a duplex-DNA-only solution were filled into quartz cells with a pathlength of 0.01-1.0 mm (Type48, Starna Scientific; GL science), respectively. The duplex-DNA-only solution contains the same DNA concentration as that in the gel sample. The proper pathlength was selected to make sure the absorbance of samples within 0.1-1.0. The absorbance at 260 nm was monitored every 0.5 °C, and the temperature was increased and decreased between 25 and 80 °C at a rate of 0.5 °C/min. Three samples were tested in each measurement.

2.6 Small-angle neutron scattering

Small-angle neutron scattering (SANS) experiments were performed by using a small- and wide-angle neutron scattering instrument, TAIKAN (BL15), in the Material and Life Science Experimental Facility (MLF) of the Japan Proton Accelerator Research Complex (J-PARC). An incident beam with a diameter of 10 mm was used to irradiate the samples in 1 mm thick quartz banjo cells. The operation power of the spallation source at our experimental time was 300 kW. All the samples used for the SANS measurements were prepared in a 25 mM sodium phosphate aqueous buffer solution at pH 7.4. The D_2O/H_2O ratio in the buffer solution was 58 vol%/42 vol%, which matches the scattering length density of the DNAs to simplify the scattering function analysis. The temperature was controlled from 25°C to 75°C with 0.1°C accuracy. SANS experiments were performed for one gel and one solution sample.

2.7 Viscoelasticity measurements

Dynamic viscoelasticity measurements were performed by using a rheometer (MCR 501, Anton Paar) with a double cylinder measuring geometry (CC-17). A lid was placed on the top of cylinder cup to avoid solvent evaporation. The heated flowing gel samples were loaded into the cylinder cup at 75°C, and the cylinder was lowered to the measurement position. Then, the samples were annealed at each measurement temperature for at least 15 min before each test. Each viscoelastic measurement was performed for three gel samples.

2.7.1 Liner viscoelasticity tests

First, to confirm the strain region showing linear viscoelasticity, strain sweep tests were performed for strains γ = 0.01-1000% at an oscillation frequency ω = 10 s^{-1} at 30-50 °C

2.7.2 Temperature sweep tests

Next, we performed temperature sweep tests to check the hysteresis after repetitive sol-gel transitions. The temperature sweep tests were performed in a temperature range between 25 and 80 °C at a rate of 0.25 °C min^{-1} at ω = 1 s^{-1}.

2.7.3 Temperature hysteresis tests

Sol-gel transition tests were performed by alternating temperatures at 25 °C and at 65 °C in turn for 7 cycles at ω = 10 s^{-1}.

2.7.4 Break and recovery tests

The break and recovery tests were performed by alternating strains at γ = 1% and at γ = 500% in turn for 10 cycles at ω = 10 s^{-1} at 25 °C.

2.7.5 Frequency sweep tests

Frequency sweep tests were performed in ω = 100–0.1 s^{-1} by applying a stain γ = 2%, which is in the linear viscoelastic region, at predefined temperatures between 45-60 °C.

2.7.6 Step-strain tests

Step-strain tests were performed by applying a step strain of γ = 2% to the samples and monitoring the time variation of the relaxation modulus $G(t)$ at predefined temperatures between 37-47 °C.

2.8 Fluorescence resonance energy transfer measurements

Fluorescence resonance energy transfer (FRET) measurements were performed using a custom-made system. The system was composed of a temperature control cuvette holder (qpod 2e, Quantum Northwest), a 470 nm LED light source (M470F3, Thorlabs), a spectrometer (FLAME-S, Ocean insight) and optical filters (excitation side: 500 nm, O.D. 4.0 short-pass filter; emission side: 500 nm, O.D. 4.0 long-pass filter).

We first filled 3mL of the phosphate buffer (pH 7.4, 25 mM) in the spectrometer cell set to a predefined temperature between 36-45 °C. Then, we dropped 30 μL of the concentrated duplex DNA solution (100 nM) into the phosphate buffer. The initial duplex DNA concentration in the phosphate buffer solution was 1 nM. We evaluated the dissociation process by monitoring the fluorescence change between 520-530 nm over time. The intensity was acquired every 0.25 s. We altered the duty cycle of the excitation light between 20-100% of one minute period to avoid photobleaching of the fluorescent dyes. Two samples were tested for each FERT measurement.

3 Sample preparation

3.1 Synthesis of star-PEG-DNA precursors

The oligonucleotides were dissolved in carbonate-bicarbonate buffer (100 mM, pH 9.5) at 15 mM, and the four-armed PEGs were dissolved in dehydrated dimethyl sulfoxide (DMSO) at 2 mM. We mixed equal volume of oligonucleotide and PEG solutions and incubated the mixed solution for three hours at room temperature with mild vertexing. The number of oligonucleotides was approximately twice of the arm number of four-arm PEGs. After the incubation, the solvent was removed from the mixture by freeze drying. The products were dissolved in DI water and purified by SEC. Star-polymer-DNA precursors were eluted at approximately 17-23 min, and unreacted oligonucleotides were eluted at 28-34 min at flow rate 1 mL/min. The collected solutions containing star-polymer-DNA precursors were evaporated by freeze drying to remove solvent.

3.2 Fabrication of star-polymer-DNA hydrogels

Star-polymer-DNA precursors with the oligo DNA and the complementary strands were dissolved in 25 mM sodium phosphate buffer (pH 7.4), respectively, at room temperature. The two precursor solutions were mixed in a test tube immersed in a hot water bath and then cooled to ambient temperature; a transparent hydrogel was formed immediately. All the experiments were performed according to the above procedure.

4 Theoretical models

4.1 Melting curve analysis of DNA with a two-state transition model

The simplest hybridization process of duplex DNA follows a two-state transition model as

$$A + B \rightleftharpoons AB \tag{S1}$$

where A and B are single-stranded DNA with complementary sequences and AB is duplex DNA. The molar concentration of A, B and AB at equilibrium are defined as $[A]_e$, $[B]_e$, $[AB]_e$, while the total molar concentration of A and B, including those forming the duplex DNA are defined as $[A]_{tot}$ and $[B]_{tot}$.

When we mix the same molar amounts of A and B in the solution, the total molar concentration of DNA strands C_T is given by

$$C_T = [A]_{tot} + [B]_{tot} = 2[A]_{tot} \tag{S2}$$

The molar fraction of duplex DNA (p) at equilibrium at temperature T is given by

$$p = \frac{[AB]_e}{[A]_{tot}} = \frac{[AB]_e}{[B]_{tot}} = 2\frac{[AB]_e}{C_T} \tag{S3}$$

In our gel system, p also denotes the crosslinking ratio because all crosslinking points are formed by the DNA duplex. Using the difference in the molar excitation coefficients of duplex DNA and single-stranded DNA at wavelength of 260 nm, p can be estimated by measuring the UV absorbance.

The absorbance $Abs(T)$ of the DNA solution at temperature T is given by the Beer–Lambert law as

$$Abs(T) = [p\epsilon_D + \{1 - p\}\bar{\epsilon}_S]C_T l \tag{S4}$$

where ϵ_D is the excitation coefficient of duplex DNA, $\bar{\epsilon}_S$ is the average excitation coefficient of single-stranded DNAs, and l is the optical pathlength. $\bar{\epsilon}_S$ and ϵ_D are assumed to be linear functions of temperature:

$$\bar{\epsilon}_S = \bar{a}_S T + \bar{b}_S \tag{S5}$$

$$\epsilon_D = a_D T + b_D \tag{S6}$$

where $\bar{a}_S$, $\bar{b}_S$, a_D and b_D are the coefficients for temperature dependence of the excitation coefficients of single-stranded DNA (average of two sequences) and duplex DNA, respectively. The values of $\bar{a}_S$, $\bar{b}_S$, a_D, b_D, and p for the DNA gel can be obtained by fitting the melting curves with eqs S4-S6.

The equilibrium constant of the two-state transition is defined as

$$K_{eq} = \frac{\frac{[AB]_e}{c^\circ}}{\frac{[A]_e}{c^\circ} \times \frac{[B]_e}{c^\circ}} = \frac{[AB]_e c^\circ}{[A]_e [B]_e} \tag{S8}$$

where c° is a standard molar concentration, whose value is typically 1 mol L^{-1}.
Using the definition of $p(T)$, K_{eq} is written as follows:

$$K_{eq} = \frac{2pc^\circ}{(1-p)^2 C_T} \tag{S9}$$

The K_{eq} is given by the standard reaction Gibbs free energy ($\Delta_r G^\circ$) as

$$K_{eq} = \exp\left(-\frac{\Delta_r G^\circ}{RT}\right) \tag{S10}$$

where R is the gas constant.
The standard reaction free energy is split into standard reaction enthalpy ($\Delta_r H^o$) and standard reaction entropy ($\Delta_r S^\circ$), and K_{eq} is written as follows.

$$\ln K_{eq} = -\frac{\Delta_r G^\circ}{RT} = -\frac{\Delta_r H^\circ}{RT} + \frac{\Delta_r S^\circ}{R} \quad \text{(S11)}$$

This plot is called the van't Hoff plot.

4.2 SANS model for four-armed block-copolymers

Scattering profiles consists of the Fourier transform of pair correlations between each two scattering elements in samples, i.e., structure factors $S(q)$. For star-polymer-DNA gels, the elements are PEG, DNA, and solvent molecules; therefore, we have totally six pair correlations: PEG-PEG, DNA-DNA, solvent-solvent, PEG-DNA, PEG-solvent, and DNA-solvent. However, in the case of small-angle scattering, probing long-range correlations, the pair correlations are negligible between solvent molecules and polymers, and between the solvent molecules themselves. Therefore, the $S(q)$ of star-polymer-DNA gel is given by a 2 × 2 square matrix as[3]:

$$\begin{pmatrix} S_{PP}(q) & S_{PD}(q) \\ S_{PD}(q) & S_{DD}(q) \end{pmatrix}^{-1} = \begin{pmatrix} S^0_{PP}(q) & S^0_{PD}(q) \\ S^0_{PD}(q) & S^0_{DD}(q) \end{pmatrix}^{-1} + \begin{pmatrix} v_{PP} & v_{PD} \\ v_{PD} & v_{DD} \end{pmatrix} \tag{S12}$$

$S^0(q)$ is the noninteracting (bare) structure factor, and v is the excluded volume parameter. The subscripts denote the pairs of elements; *P* indicates PEG and *D* indicates DNA. The bare structure factor is given by the pair correlations inside the star-polymer-DNA precursor, i.e., form factors $P(q)$ as:

$$S^0_{PP}(q) = N\varphi V_P P_{PP}(q) \tag{S13}$$

$$S^0_{PD}(q) = N\varphi\sqrt{V_P V_D} P_{PD}(q) \tag{S14}$$

$$S^0_{DD}(q) = N\varphi V_D P_{DD}(q) \tag{S15}$$

Here, N is the degree of polymerization of a star-polymer-DNA precursor, φ is the polymer volume fraction of the star-polymer-DNA precursors, V_P and V_D are the segment volumes of PEG and DNA.

Here, we roughly assume that the star-polymer-DNA precursor is a multi-armed star block copolymer with a segment length b following Gaussian statistics. The detailed expression of the form factors of the simplified star-polymer-DNA precursor is given by[3,4]

$$P_{HH}(q) = g(2-g)h\left(\frac{1-f}{g}, u\right) + \frac{g(g-1)}{2} h\left[\frac{2(1-f)}{g}, u\right] \tag{S16}$$

$$P_{DD}(q) = gh\left(\frac{f}{g}, u\right) + \frac{g(g-1)}{2}\left\{h\left(\frac{2}{g}, u\right) - h\left[\frac{2(1-f)}{g}, u\right] - 2h\left[\frac{2-f}{g}, u\right]\right\} \quad \text{(S17)}$$

$$P_{HD}(q) = \frac{g(g-2)}{2}\left[h\left(\frac{1-f}{g}, u\right) - h\left(\frac{1}{g}, u\right)\right] - \frac{g}{2}h\left(\frac{f}{g}, u\right) + \frac{g(g-1)}{2}\left[h\left(\frac{2-f}{g}, u\right) - h\left(\frac{2(1-f)}{g}, u\right)\right] \quad \text{(S18)}$$

Here, g is the number of arms per precursor, e.g., $g = 4$ in this study, and f is the length fraction of DNA per arm. $h(f, u)$ is the Leibler function[5] and is given by

$$h(f, u) = \frac{2[fu + \exp(-fu) - 1]}{u^2} \quad \text{(S19)}$$

where

$$u = \frac{q^2 N b^2}{6} \quad \text{(S20)}$$

For the star-polymer-DNA precursors with N_P of PEG segments per precursor and N_D of DNA segments per arm, the total polymerization degree N and the DNA fraction per arm f are given as:

$$N = N_p + 4N_D \quad \text{(S21)}$$

$$f = \frac{N_D}{\frac{N_P}{4} + N_D} \quad (S22)$$

The absolute scattering intensity for the star-polymer-DNA gel is given by

$$I(q) = \Delta\rho_P^2 S_{PP}(q) + \Delta\rho_D^2 S_{DD}(q) + 2\Delta\rho_P \Delta\rho_D S_{PD}(q) \quad \text{(S23)}$$

where $\Delta\rho$ is the difference of the scattering length densities between polymer chains and solvent molecules.

Because $\Delta\rho_D = 0$ in this study, the absolute scattering intensity can be simplified as:

$$I(q) = \Delta\rho_P^2 S_{PP}(q) \quad \text{(S24)}$$

The detailed expression of $S_{PP}(q)$ is as follows S25:

$$S_{PP}(q) = \frac{S_{PP}^0 + (v_{DD})\{S_{PP}^0(q)S_{DD}^0(q) - [S_{PD}^0(q)]^2\}}{1 + v_{PP}S_{PP}^0 + v_{DD}S_{DD}^0 + 2v_{PD}S_{PD}^0 + (v_{PP}v_{DD} - v_{PD}^2)(S_{PP}^0S_{DD}^0 - [S_{PD}^0(q)]^2)} \quad \text{(S25)}$$

According to the Flory-Huggins theory[6], the v parameters are given by

$$v_{PP} = \frac{1}{V_s}\left(\frac{1}{1-\varphi} - 2\chi_{PS}\right) \quad \text{(S26)}$$

$$v_{DD} = \frac{1}{V_s}\left(\frac{1}{1-\varphi} - 2\chi_{DS}\right) \quad \text{(S27)}$$

$$v_{PD} = \frac{1}{V_s}\left(\frac{1}{1-\varphi} - \chi_{PS} - \chi_{DS} + \chi_{PD}\right) \quad \text{(S28)}$$

where V_s is the volume of a Flory lattice (here we used the volume of the water molecule), and χ is the Flory interaction parameter between the elements *i* and *j*. The subscripts denote PEG for P, DNA for D, and solvent molecules for S.

The model scattering function is obtained by combining the equations S13-15, S24, and S26-28. There are total nine linear dependent parameters in the model scattering function: N_P, N_D, V_S, V_P, V_D, b, χ_{PS}, χ_{DS}, and χ_{PD}. To simplify the model function fitting, we assumed that PEG and DNA are the Gaussian chains with the same segment lengths and the same segment volumes. In the fitting analysis of the scattering profiles, we used N_D, χ_{PS}, χ_{DS}, and χ_{PD} as fitting parameters and fixed N_P, V_S, V_P, V_D, and b as follows: N_P = 909 Å^3, V_S = 30 Å^3, V_P = 65 Å^3, V_D = 65 Å^3, and b = 5.89 Å[7].

4.3 Maxwell model for viscoelasticity

The Maxwell model is one of the simplest models for viscoelastic phenomena, combining a viscous element (dashpot) and an elastic element (spring). When applying a constant strain to a Maxwell element, the spring element is stretched and the dashpot element remained unchanged in the beginning, yielding an initial shear modulus G_0. As time passes, the dashpot moves to relax the applied stress. This relaxation process is described by a single exponential decay function as:

$$G(t) = G_0 \exp\left(-\frac{t}{\tau_R}\right) \tag{S29}$$

where $G(t)$ is the shear modulus at time t and τ_R is the characteristic relaxation time.

In contrast, when applying an oscillation strain to the Maxwell element, the elastic modulus is measured by two separate components: the storage modulus G', denoting the elastic characteristics, and loss modulus G'', denoting the viscous characteristics. The detailed expressions are given as a function of oscillation frequency ω and τ_R:

$$G' = G_0 \frac{\omega^2 \tau_R^2}{\omega^2 \tau_R^2 + 1} = \begin{cases} \omega^2, & for\ \omega\tau_R \ll 1 \\ \omega^0, & for\ \omega\tau_R \gg 1 \end{cases} \tag{S30}$$

$$G'' = G_0 \frac{\omega \tau_R}{\omega^2 \tau_R^2 + 1} = \begin{cases} \omega^{-1}, & for\ \omega\tau_R \ll 1 \\ \omega^1, & for\ \omega\tau_R \gg 1 \end{cases} \tag{S31}$$

Note that the crossover point of the G' and G'' profiles is τ_R[8].

4.4 Analysis model for stress relaxations

To obtain the longest relaxation time τ_R in the stress relaxation curves. We fitted $G(t)$ in step-strain tests with the following equation.

$$G(t) = G_0\left((1-A)\exp\left[-\left(\frac{t}{\tau_{fast}}\right)^{\beta}\right] + A\exp\left(-\frac{t}{\tau_R}\right)\right) \quad \text{(S32)}$$

where $G(t)$ is the shear modulus at time t, G_0 is initial shar modulus, A is the ratio of the latest stress relaxation in the stress relaxation curve, τ_{fast} is the characteristic relaxation time of fast relaxation modes, and β is a stretched exponent. The fast relaxation may be attributed to the entanglement between DNA and PEG polymers and the rotational motion of the DNA.

4.5 Determination of the thermodynamic potentials of DNA by T_m

Regarding to the thermodynamic potentials of DNA, e.g., $\Delta_r H^o$, $\Delta r S^o$ and $\Delta_r G^o$, in addition to the melting curve fitting analysis, we performed more precise estimations by using the dependence of the melting temperature T_m on the total DNA concentration C_T, so-called T_m^{-1} vs $C_T/4$ analysis[9]. The reason for using this method was to increase the number of data points and improve the estimation accuracy.

By the definition of T_m, i.e., the temperature where half of the duplex DNA dissociates, $p(T_m) = 0.5$. Substituting $p(T_m)$ into equation S9, we obtain

$$K_{eq} = \frac{4c^\circ}{C_T} \tag{S33}$$

In combination with relationship between the standard reaction Gibbs free energy and the equilibrium constant, we have:

$$\exp\left(-\frac{\Delta_r G^\circ(T_m)}{RT_m}\right) = \frac{4c^\circ}{C_T} \tag{S34}$$

$$\frac{\Delta_r H^\circ - T_m \Delta_r S^\circ}{RT_m} = -\ln\frac{4c^\circ}{C_T} \tag{S35}$$

By organizing the above equation, we have the so-called T_m^{-1} vs $C_T/4$ plot:

$$\frac{1}{T_m} = \frac{R}{\Delta_r H^\circ}\ln\frac{C_T}{4c^\circ} + \frac{\Delta_r S^\circ}{\Delta_r H^\circ} \tag{S36}$$

4.6 Dissociation kinetics of duplex DNA measured with FRET technique

When a duplex DNA solution is added in a large volume of buffer solution, the duplex dissociation is the primary process in a short time, and we can exclusively evaluate the dissociation kinetics. Assuming that the DNA dissociation follows the two-state transition model, the chemical equation of the dissociation process is:

$$AB \rightarrow A + B \tag{S37}$$

When we monitor the dissociation process using FRET technique, the fluorescence intensity $I(t)$ from the DNA solution is given by

$$I(t) = F_{AB}[AB] + F_A[A] \tag{S38}$$

where F_{AB} and F_A are the molar fluorescence coefficients of the duplex DNA and the oligo DNA A. Equation S38 does not have a term for DNA B because it does not carry flutophone.

The normalized molar concentration of the DNA duplex (α) is defined as:

$$\alpha = \frac{[AB]}{[AB]_0} \tag{S39}$$

Here, $[AB]_0$ is initial concentration duplex DNA, which was 1 nM in this study. Using α, $I(t)$ is written as:

$$I(t) = \alpha F_{AB}[AB]_0 + (1 - \alpha)F_A[AB]_0 \tag{S40}$$

By rearranging Equation S40 for α, we have:

$$\alpha = \frac{I(t) - F_A[AB]_0}{F_{AB}[AB]_0 - F_A[AB]_0} \tag{S41}$$

While $F_{AB}[AB]_0$ is the initial fluorescence intensity, i.e., $I(0)$, $F_A[AB]_0$ is the fluorescence intensity of a solution with fluorophore-labeled DNA only because $F_A[AB]_0 = F_A[A]_{tot}$. By measuring $I(t)$, $F_{AB}[AB]_0$ and $F_A[A]_{tot}$ separately, we can convert the fluorescent intensity to the normalized duplex DNA concentration α.

By assuming that the dissociation process of the duplex DNA is a first-order reaction, the integrated rate law of the dissociation process is:

$$[AB] = [AB]_0 \exp(-k_d t) \tag{S42}$$

By taking the logarithm of each side in the above equation and substituting equation S39 to it, we obtain the relation between α and k_d.

$$\ln \alpha = -k_d t \tag{S43}$$

The k_d values can be obtained by fitting the time variation of α with equation S43.

5 Supplementary results

5.1 Design of the DNA sequence by computation

In designing the DNA sequences, we focused on whether the DNA duplexes exhibit ideal two-state transition. We currently do not have a straightforward strategy to search for the best sequences; we need to randomly test the candidates. In current work, we first tested the simplest sequence pair, e.g., polyA-polyT, but the simulation results for the melting curve and equilibrium pair probability matrices both suggested complicated structures. Next, we randomly designed several sequences and performed the same tests. Finally, we chose the sequence pair that shows clear two-state transition and proper melting temperature for building the gels. Here, we show several test results.

This work

Strand A: 5′-TCGCAACAATAACTGA-3′
Strand B: 5′-TCAGTTATTGTTGCGA-3′

Sequence pair 1

Strand A: 5′-AAAAAAAAAAAAAAAA-3′
Strand B: 5′-TTTTTTTTTTTTTTTT-3′

Sequence pair 2

Strand A: 5′-TCGTACATTAGTACGT-3′
Strand B: 5′-ACGTACTAATGTACGA-3′

Sequence pair 3

Strand A: 5′-TCGATCTA-3′
Strand B: 5′-TAGATCGA-3′

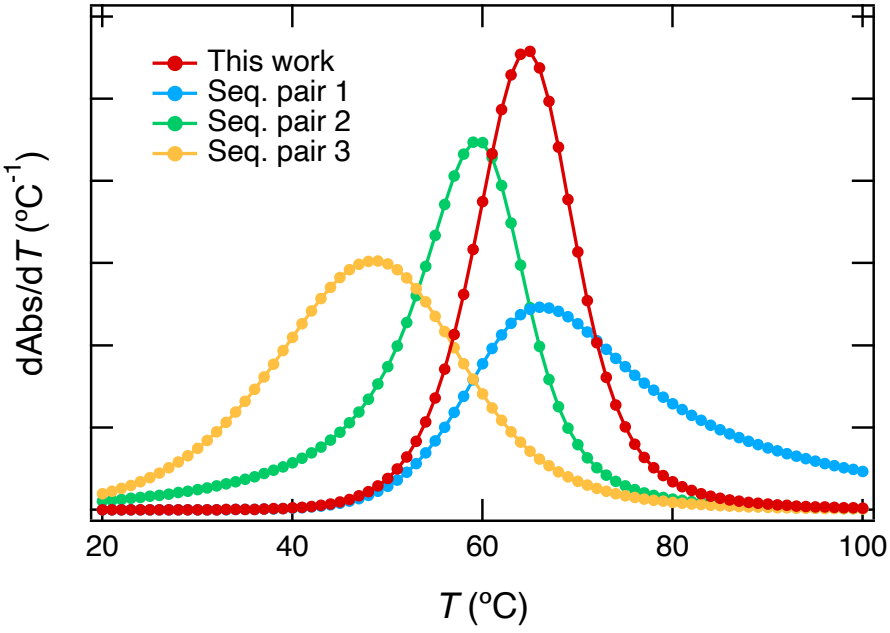

Figure S1. The first derivatives of the melting curves computed for the sequences designed in this work and a few examples for inappropriate sequences. The melting curves were computed using DINAmelt (http://www.unafold.org/hybrid2.php) at a duplex DNA concentration of 4 mM and a sodium concentration of 37.5 mM, which counts all sodium ions from the phosphate buffer. The first derivative curve for the sequences used in this study is Gaussian-like with a peak near T_m, suggesting that the DNA transition showed a simple two-state transition from a duplex to single strands. However, the first derivative curve of the sequence pair 1 (polyA-polyT) and sequence pair 2 (known to have a stem loop) exhibited unsymmetric shapes with either a long tail or a peak fronting. These unsymmetric melting curve suggest the non-ideal transitions from the duplexes to single stranded DNA. The derivative curve of the sequence pair 3 (shorter oligo DNA, 8 mer) has a symmetric shape, but its T_m is much lower than the sequence used in this work; the low T_m will deteriorate the stability of the DNA gels at physiological conditions.

a

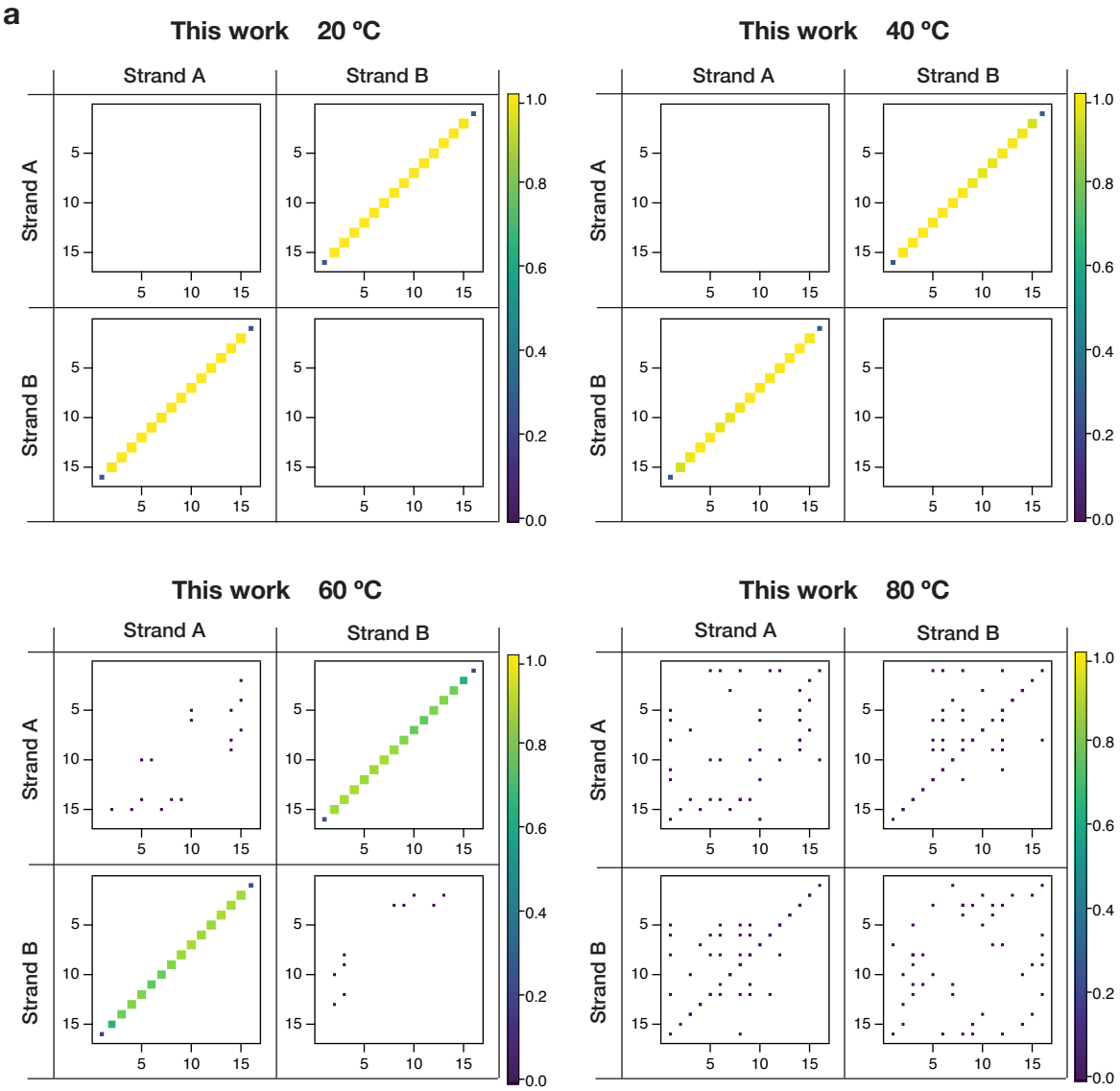
This work 20 °C
This work 40 °C
This work 60 °C
This work 80 °C
Strand A
Strand B
5
10
15
1.0
0.8
0.6
0.4
0.2
0.0

b

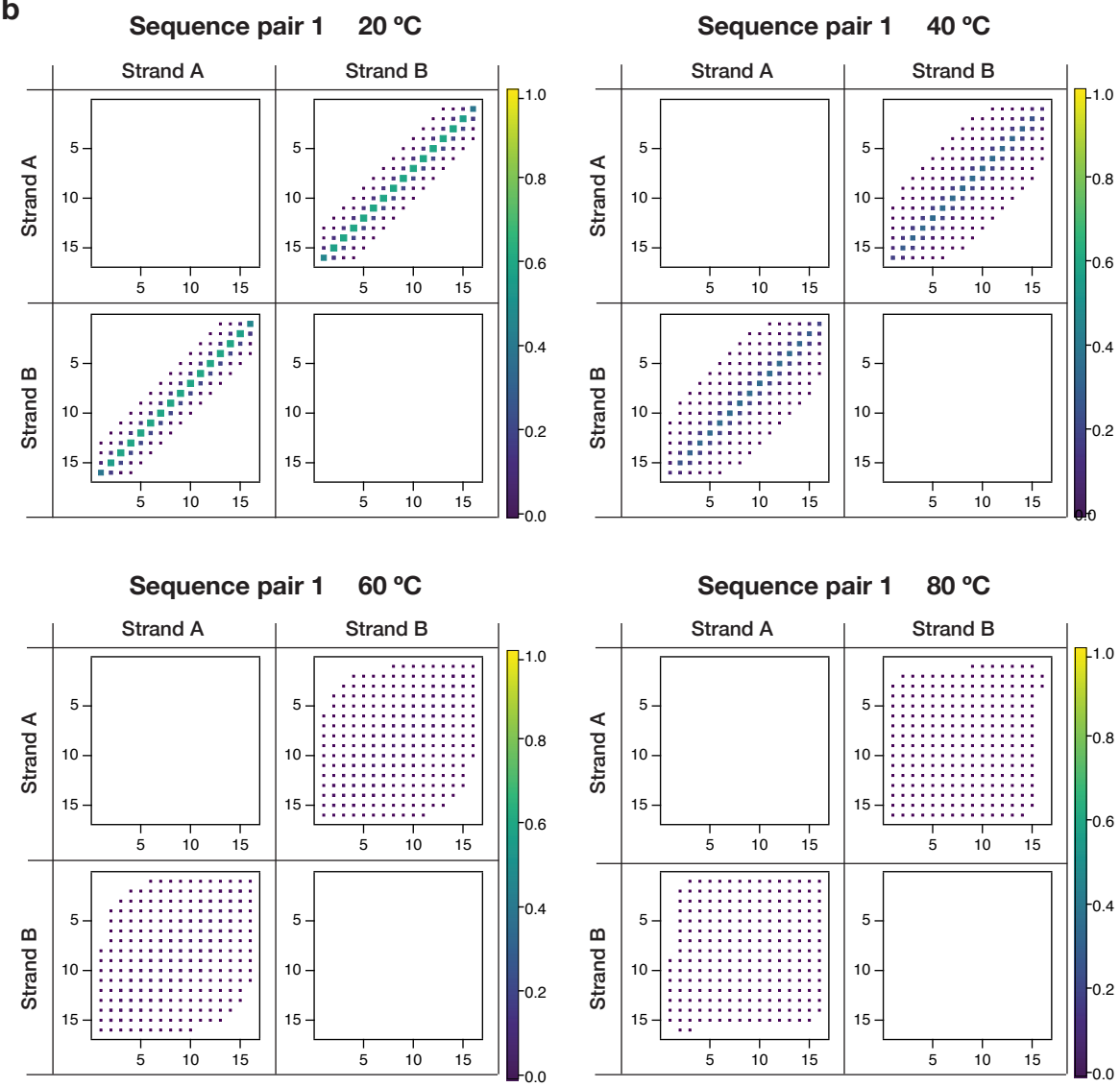
Sequence pair 1 20 ºC
Sequence pair 1 40 ºC
Sequence pair 1 60 ºC
Sequence pair 1 80 ºC
Strand A
Strand B
5
10
15
0.0
0.2
0.4
0.6
0.8
1.0

c

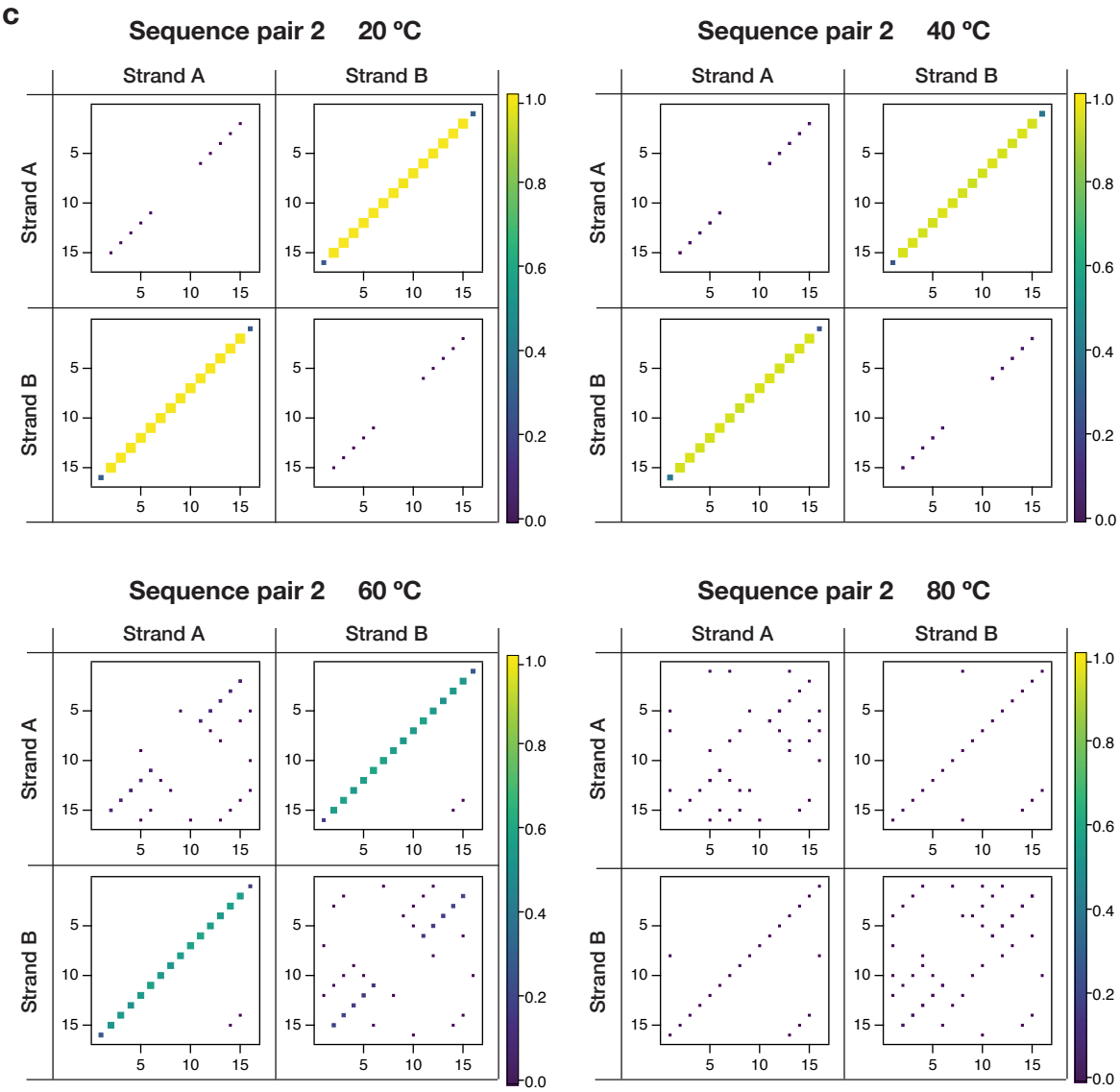
Sequence pair 2 20 °C
Sequence pair 2 40 °C
Sequence pair 2 60 °C
Sequence pair 2 80 °C
Strand A
Strand B
5
10
15
1.0
0.8
0.6
0.4
0.2
0.0

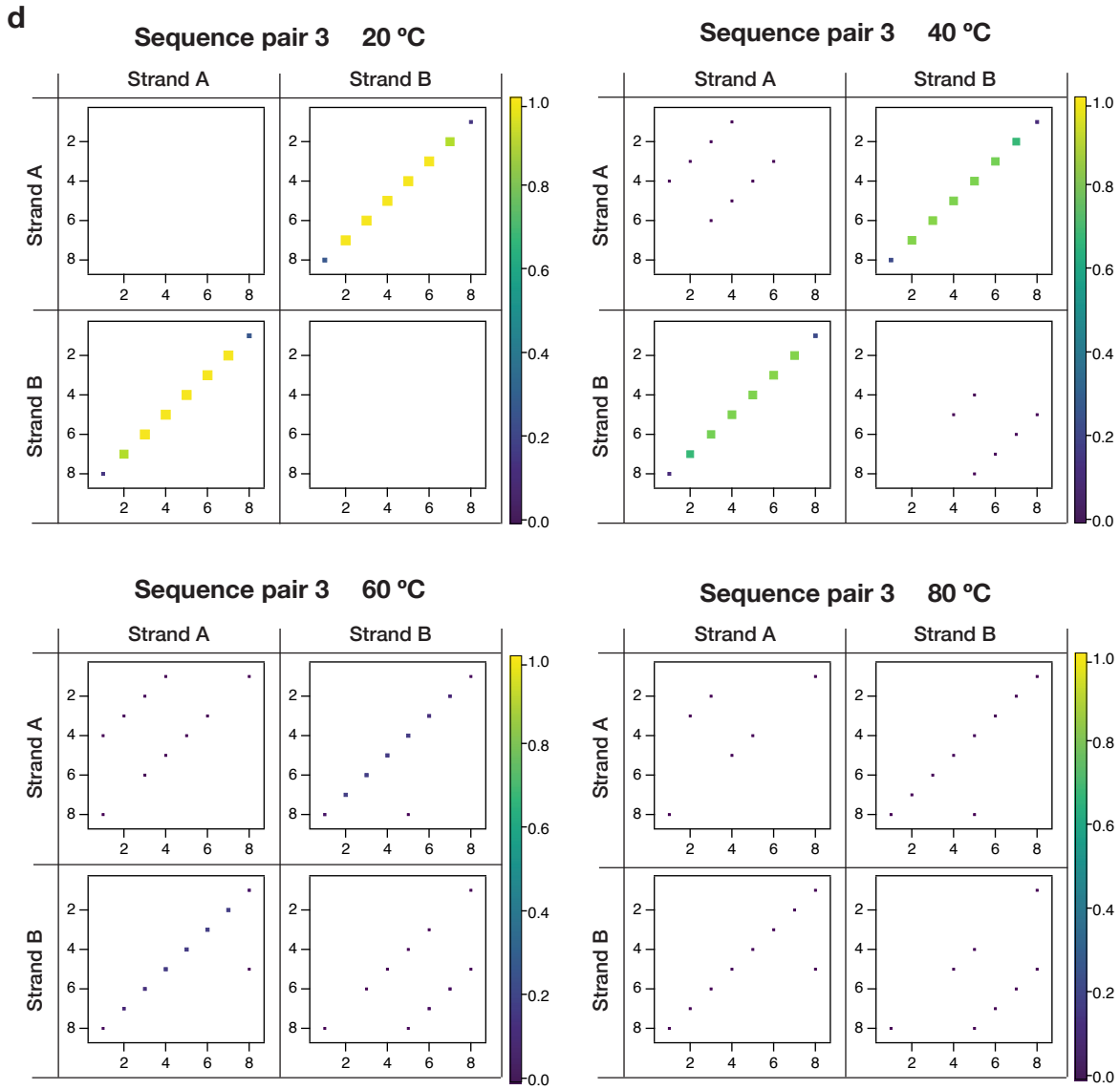

Figure S2. The equilibrium pair probability matrices for the designed sequences in this work and the examples of inappropriate sequences (the sequences are the same as in Fig S1). The pair probability matrices were calculated using NUPACK [10] from 20 °C to 80 ºC at the sodium concentration of 50 mM. The sodium concentration in the calculation was slightly higher than the actual concentration (37.5 mM) due to the limitation of the software. The colored marks in each matrix represents the pair probabilities for the *i*th base in a DNA strand hybridizing with *j*th base in another DNA strand. The base index starts from 5'-terminal and ends at 3'-terminal. The size of marks with low probability was reduced to improve the visibility. For sequences showing the ideal two-state transition, we should only observe the diagonal elements and only in the combination of strand A vs strand B and strand B vs strand A. While the sequence pair used in this work and the sequence pair 3 (short oligo DNA, 8 mer)

could undergo the ideal two-state transition, the sequence pairs 1 and 2 would have complicated hybridization structures.

5.2 Characterization of star-polymer-DNA precursors

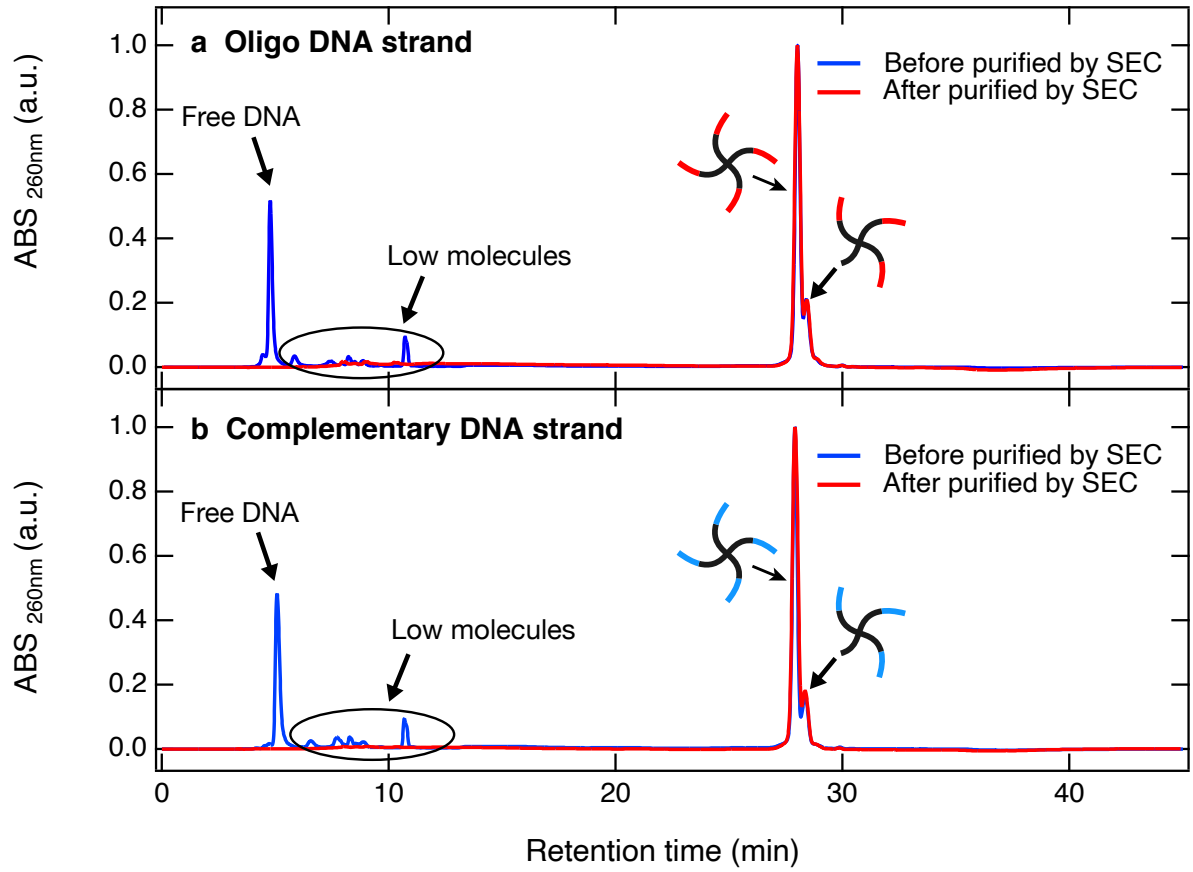

Figure S3. The reversed-phase chromatograms for star-polymer-DNA precursors used in this study. a, Chromatogram of star-polymer-DNA precursors with the oligo DNA sequence, **b**, the chromatograms with the complementary sequence. The blue curves show crude products and the red curves show purified products after the purification by SEC.

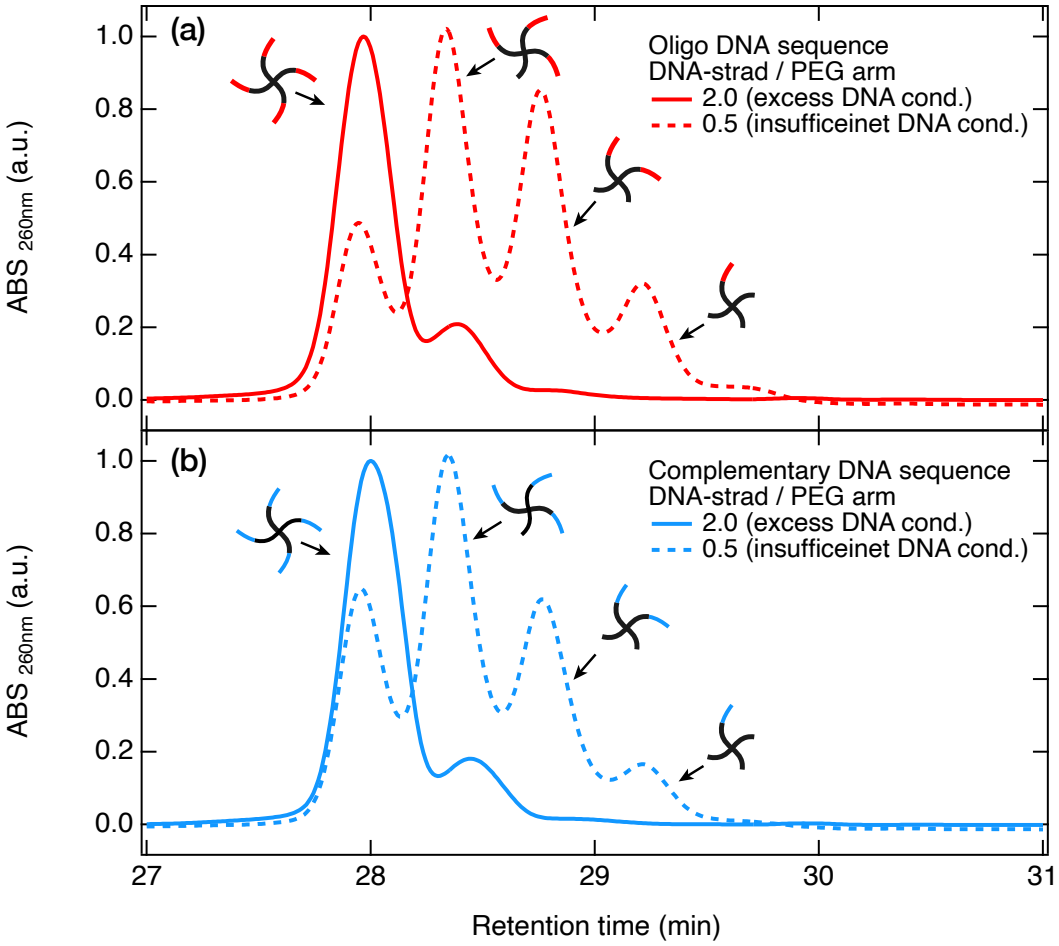

Figure S4. Magnified view of the reversed-phase chromatograms for star-polymer-DNA precursors. a, Chromatogram of star-polymer-DNA precursors with oligo DNA sequence. **b**, Chromatogram of star-polymer-DNA precursors with complementary sequences. The solid curves show the precursors synthesized at a DNA-strand/PEG-arm molar ratio = 2 (excess DNA condition), while the dashed curves show the precursors synthesized at a DNA-strand/PEG-arm molar ratio = 0.5 (insufficient DNA condition). Insufficient DNA conditions are displayed to assess the peak positions of the star-polymer-DNA precursors with 4, 3, 2 and 1 DNA strands. Totally unreacted four-armed PEGs with zero DNA strands do not appear on the chromatogram because PEG do not have absorbing groups at 260 nm. However, as for the star-polymer-DNA precursors synthesized at the excess DNA conditions, the amount of the fully unreacted PEGs should be negligible.

Table S1. Number fraction of the precursors with 1, 2, 3 and 4-DNA conjugations and the average modification conversion per arm of the four-armed PEG estimated from reversed-phase chromatogram. The values here were for the precursors synthesized under excess DNA conditions.

	Number fraction of precursors with f'-DNA				*Average conversion per arm of PEG*
	1-DNA	*2-DNA*	*3-DNA*	*4-DNA*	
Sense strands	0%	0%	23%	77%	*94.3%*
Antisense strands	0%	0%	20%	80%	*94.9%*

The number of DNA strands in each peak of the chromatogram in Fig S3 can be estimated as

$$Number\ of\ DNA\ in\ the\ peak = \frac{Peak\ area}{Abs\ per\ DNA} = \frac{Peak\ area}{\varepsilon l N_A}$$

where ε is the molar absorption coefficient of DNA, N_A is Avogadro's constant, and l is the pathlength of a detection cell.

To obtain the number of precursors in each peak, we need to normalize the peak area with the number of DNA conjugations in the corresponding peak (for example, when the number of precursors is the same in all peaks, the peak for 4-DNA precursors has 4 times larger peak area than the peak of 1-DNA precursors):

$$Number\ of\ precuser\ in\ the\ peak = \frac{Number\ of\ DNA\ per\ peak}{f'} = \frac{Peak\ area}{f'\varepsilon l N_A}$$

where *f'* is the number of DNA strand conjugated to a four arm precure. The *f'* value is different for each peak and its value can be estimated using the insufficient DNA conditions as shown in Fig S4.

The total number of DNA strands from all peaks is given as:

$$Total\ number\ of\ DNA = \sum_{f\prime=1}^{4} Number\ of\ DNA\ in\ the\ peak$$

Following the same scheme, the total number of four-armed precures is given by:

$$Total\ number\ of\ precuser = \sum_{f\prime=1}^{4} Number\ of\ precuser\ in\ the\ peak$$

The number fraction of the precursors with 1-DNA, 2-DNA, 3-DNA, and 4-DNA conjugations can be estimated as:

$$Number\ fraction\ of\ precursors\ with\ f'DNA = \frac{Number\ of\ precursors\ in\ the\ peak}{Total\ number\ of\ precuser}$$

Finally, the average modification conversion of DNA per *arm* of the four-armed precursor is given by:

$$Average\ conversion\ per\ arm\ of\ precuser = \frac{Total\ number\ of\ DNA}{Total\ number\ of\ precuser\ arms}$$

$$= \frac{Total\ number\ of\ DNA}{4 \times (Total\ number\ of\ precuser)}$$

5.3 Melting curve analysis of DNA gels and DNA-only solutions

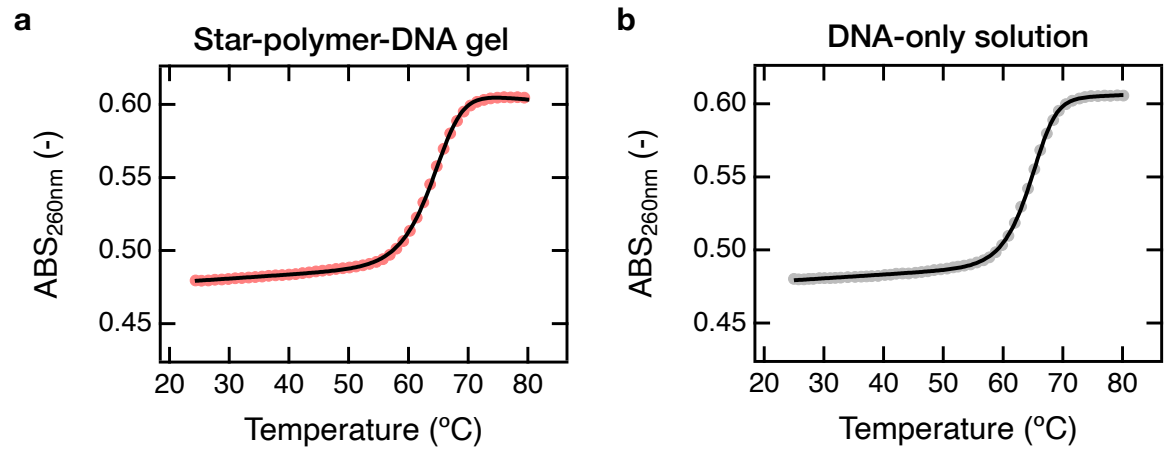

Figure S5. Fitting analysis for the melting curves using equations S4-S6. a, The star-polymer-DNA gel, and **b**, DNA-only solution with almost the same DNA concentration as in the gel. The melting curve of the DNA-only solution was vertically scaled by a factor of 1.078 to correct the slight difference in the DNA concentration.

The values of $\bar{a}_S$, $\bar{b}_S$, a_D, b_D, and p for the DNA gel can be obtained by fitting the melting curves with eqs S4-S6. The estimated p value of the DNA gel at each temperature were:

Table S2. The duplex fraction p at various temperatures.

Temperature (°C)	Duplex ratio, p
24.3	1.00
34.9	1.00
45.0	0.99
55.2	0.96
60.2	0.79
65.3	0.35
69.8	0.06
75.4	0.00
80.0	0.00

Table S3. Fitting results of the melting curves and the simulated parameters using the DNA calculator DINAMelt[1]. $\Delta_r H^o$ and $\Delta_r S^o$ for the gel and solution samples were calculated by fitting $\ln K_{eq}$ vs $1/T$ with the van't Hoff equation. K_{eq} was calculated from p using eqs S9.

	T_m (ºC)	$\Delta_r H^o$ (kJ/mol)	$\Delta_r S^o$ (kJ/mol)
Star-polymer-DNA gel	63.2	−578	−1.5
DNA-only solution	62.8	−615	−1.71
DNA calculator (DINAMelt)	64.7	−549	−1.63

5.4 Hysteresis verification after repetitive sol-gel transitions

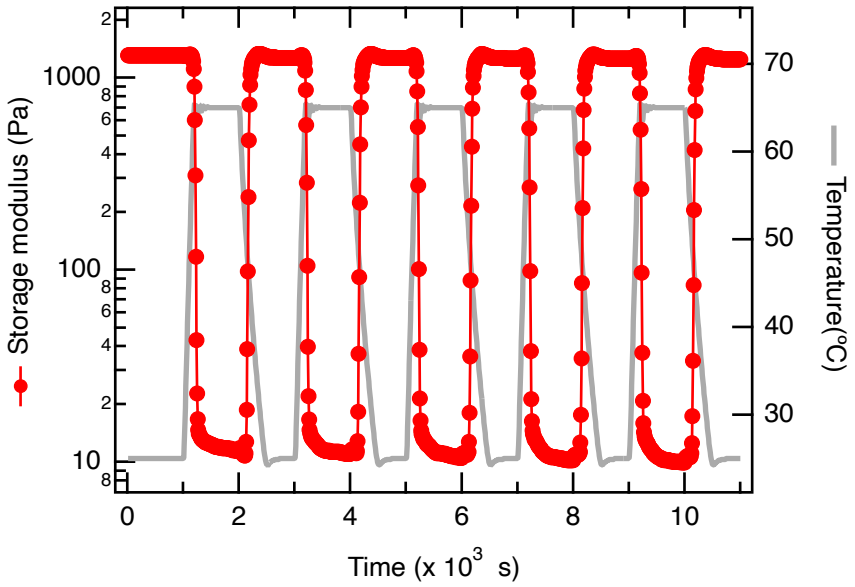

Figure S6. Hysteresis of the star-polymer-DNA gel after repetitive sol-gel transitions by changing temperatures. At low temperatures (25 °C), DNA strands forms duplex and the star-polymers DNA formed a polymer network. At high temperatures (65 °C), the duplex dissociated, and the network changed to a solution. No hysteresis was observed even after six cycles.

5.5 Structural analysis of DNA gels

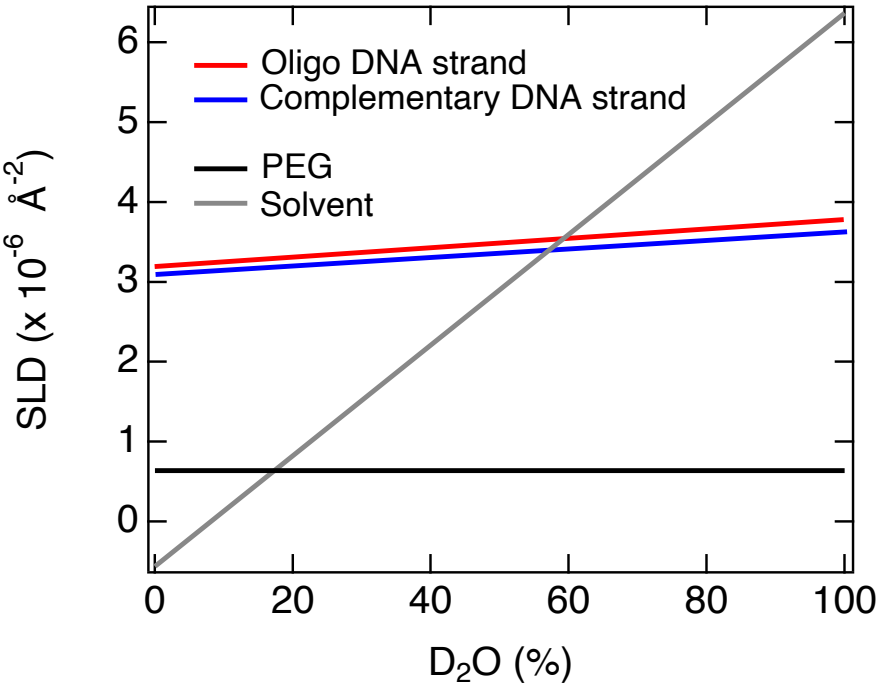

Figure S7. Neutron scattering length density (SLD) for the DNA, PEG and buffer solvent at different D_2O concentrations. The SLD values were calculated using literature values[11]. The increase in the SLD of DNA is due the exchange between the labile hydrogen of the DNA and that in the solvent. SANS measurements were performed in 60% D_2O sodium phosphate buffer, whose SLD matches that of the DNA.

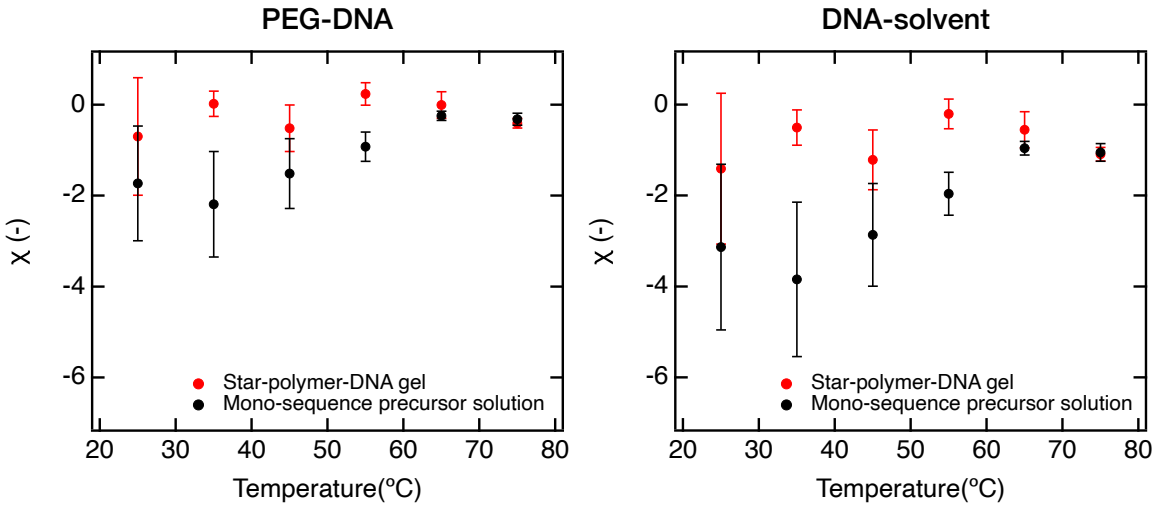

Figure S8. Temperature dependence of Flory intercalation parameter χ relating with DNA. The χ values were estimated from the SANS measurements using the model function mentioned in the SANS section. The error bars are the standard deviation of the fit analysis with our scattering model. Because the constructed model does not contain the terms for the electrostatic interactions of DNA, the χ values relating to the DNA also contains the effect of the electrostatic interactions, resulting in anormal values.

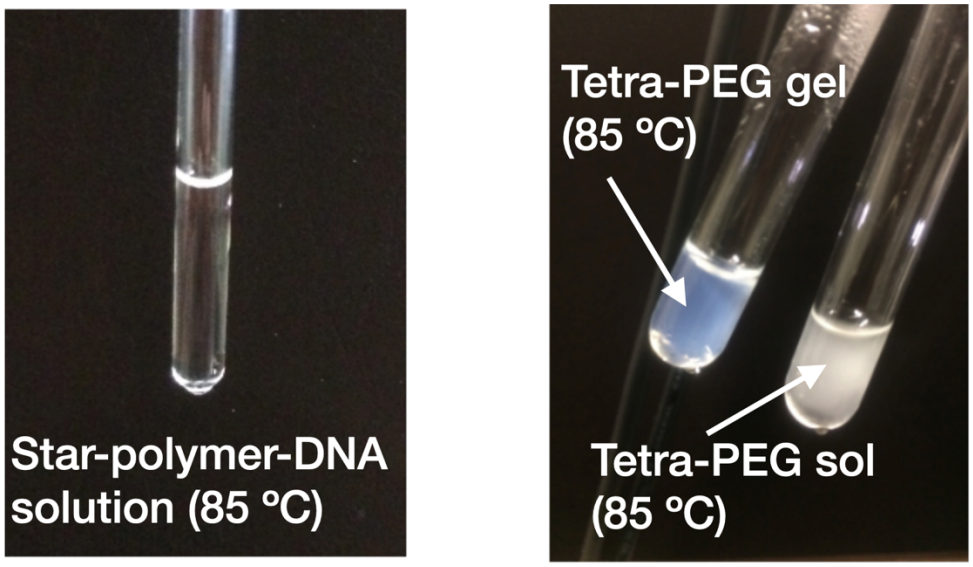

Figure S9. Photographs of the star-polymer-DNA solution, and a four-armed PEG gel and the corresponding solution in the 25 mM phosphate buffer at 85 ºC. While the solution and gel consisting of only the four-armed PEG was turbid, the star-polymer-DNA solution (DNA conjugated four-armed PEG) was transparent, suggesting that the solubility of PEG polymers was enhanced by the conjugation with DNA.

5.6 Viscoelastic properties of a DNA gel

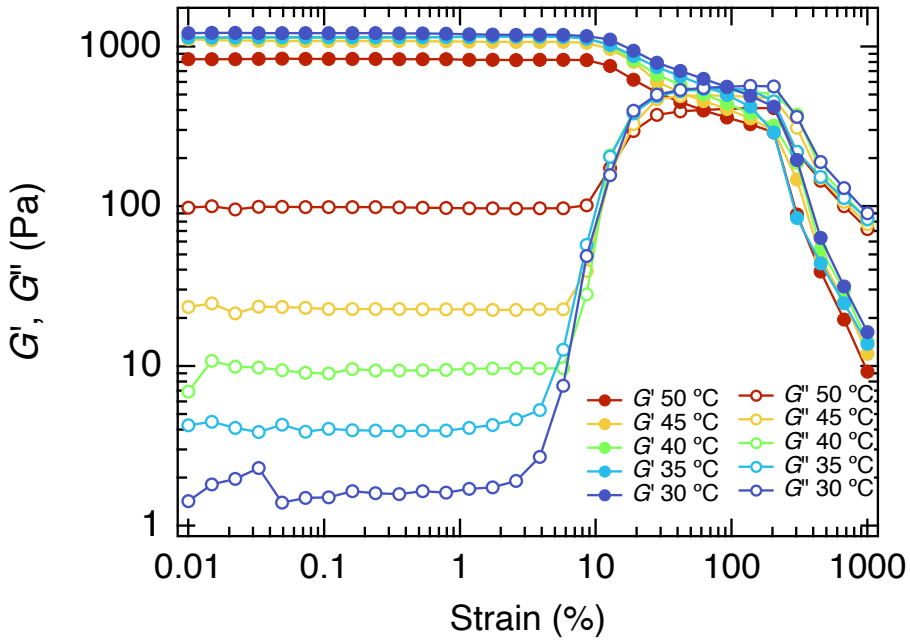

Figure S10. Strain sweep measurements were performed to confirm the linear viscoelastic region for star-polymer-DNA gels. *G*' and *G*" do not depend on the strain in the linear viscoelasticity region, corresponding to the strain smaller than 2%.

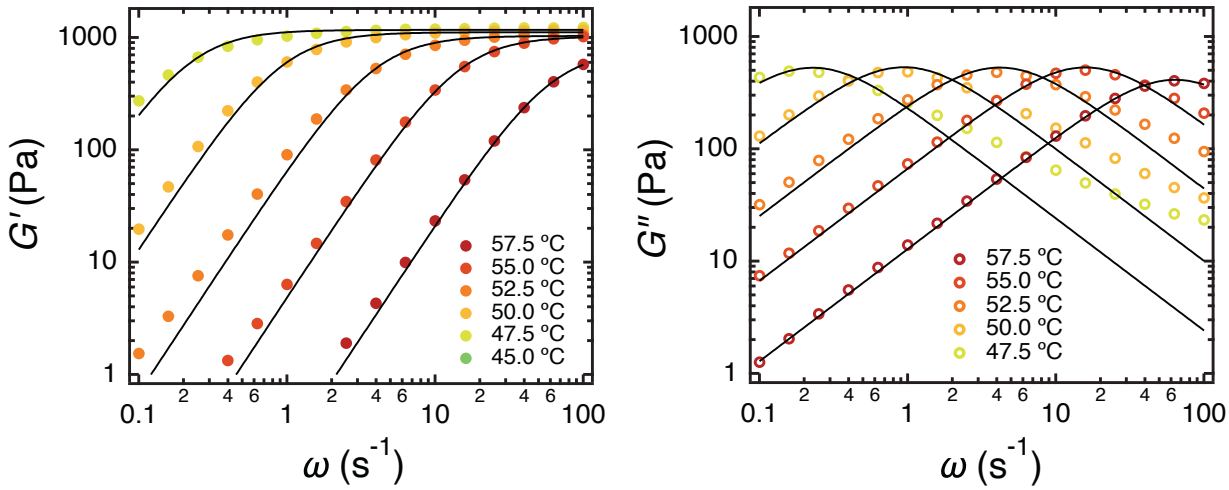

Figure S11. Temperature dependence of the *G*' and *G*" profiles measured by oscillatory tests. The black solid lines are the fitting results for a single Maxwell model (equations 30 and 31).

5.7 FRET analysis of DNA duplexes

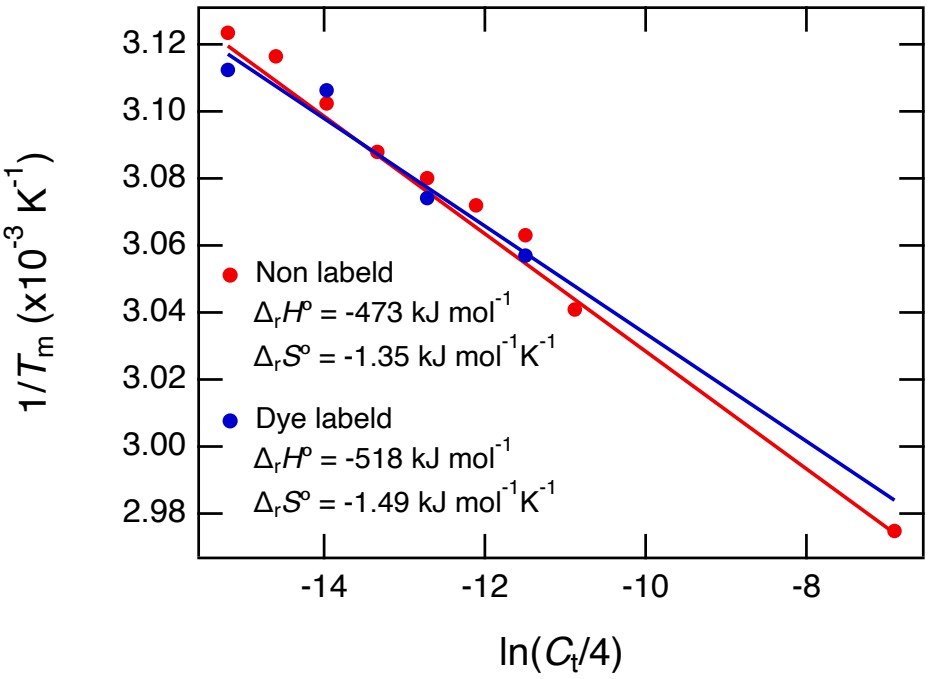

Figure S12. The plots of reciprocal melting temperatures (T_m) versus total concentrations of DNA (C_T) used to confirm the change in thermodynamic potentials before and after the labeling with fluorophores (FAM) and quenchers (BHQ1). The change in the standard thermodynamic potentials for the duplex formation after dye labeling was within 10%, indicating that the dye labeling affects little on the thermodynamic properties of DNA. Because the kinetics rate constants are deeply involved with the thermodynamic potentials, the dissociation process was likely affected little as well.

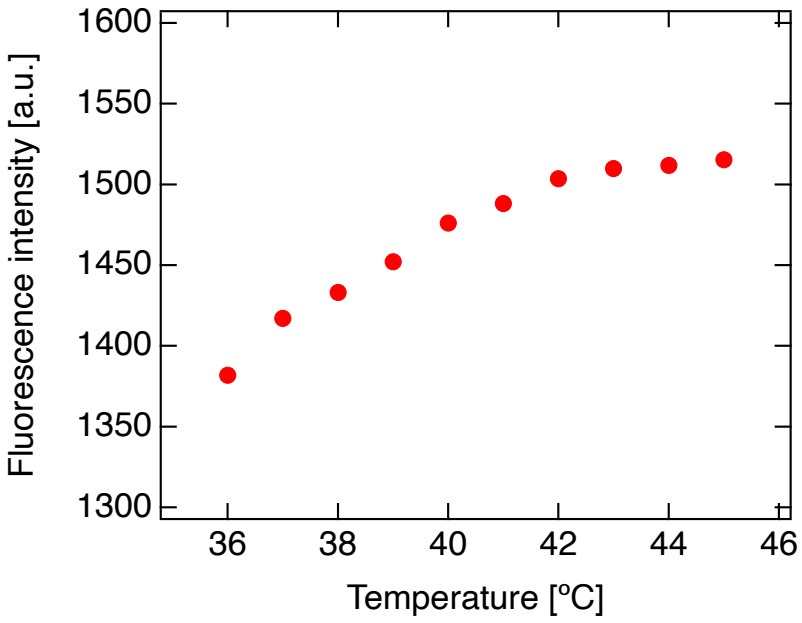

Figure S13. Temperature dependence for fluorescein (FAM) attached to the 3' end of single-stranded oligo DNA. The DNA concentration was 1 nM. As mentioned in section 4.6, the profiles for the observed fluorescent intensities were normalized by these values to estimate the duplex concentrations.

5.8 Eyring plots for gel stress relaxation time and duplex DNA dissociation time

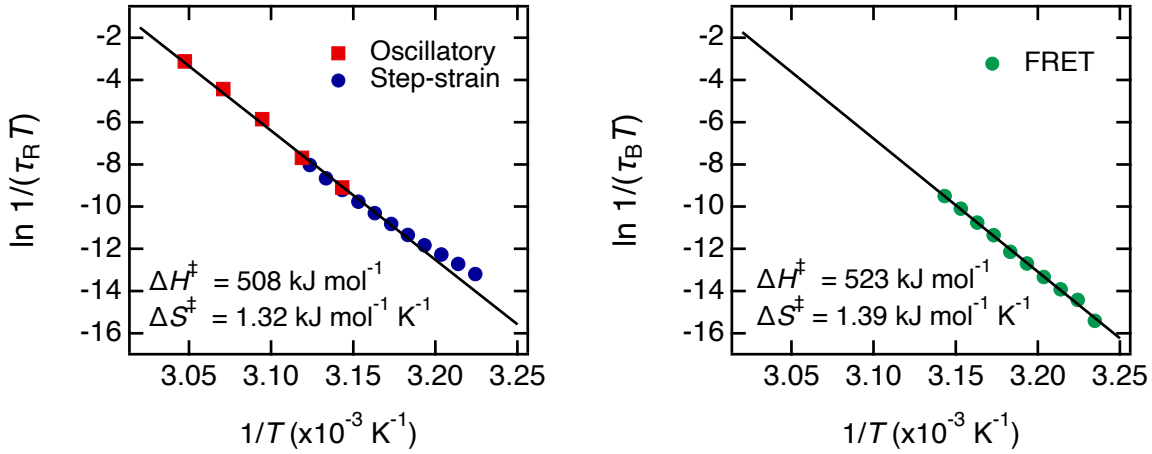

Figure S14. The Eyring plots of the τ_R and τ_d. The solid lines show the fitting results of the Eyring equation, $1/\tau = (k_BT/h)\exp(-\Delta G^{\ddagger}/RT) = (k_BT/h)\exp(-\Delta H^{\ddagger}/RT+\Delta S^{\ddagger}/R)$. Here, k_B is the Boltzmann constant, h is the Planck constant, $\Delta G^{\ddagger}$ is the Gibbs energy of activation, $\Delta H^{\ddagger}$ is the enthalpy of activation and $\Delta S^{\ddagger}$ is the entropy of activation.

5.9 Comparison of DNA duplexes with other dynamic crosslinkers

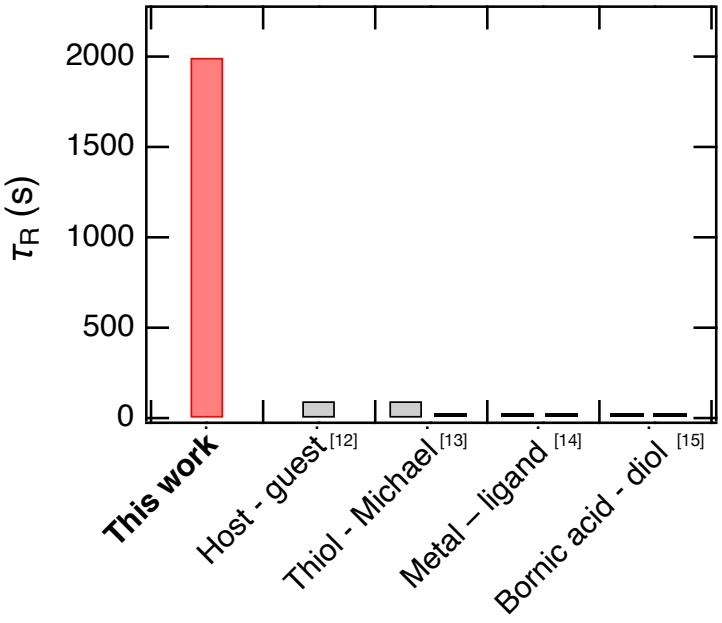

Figure S15. τ_R of the dynamically crosslinked polymer materials. The τ_R values were measured at pH 7-7.5 and 25-37 ºC.

6 References

[1] N. R. Markham, M. Zuker, *Nucleic Acids Res* 2005, *33*, W577.

[2] J. N. Zadeh, C. D. Steenberg, J. S. Bois, B. R. Wolfe, M. B. Pierce, A. R. Khan, R. M. Dirks, N. A. Pierce, *J Comput Chem* 2011, *32*, 170.

[3] M. Ohira, Y. Tsuji, N. Watanabe, K. Morishima, E. P. Gilbert, X. Li, M. Shibayama, *Macromolecules* 2020, *53*, 4047.

[4] K. Mortensen, A. L. Borger, J. J. K. Kirkensgaard, *Phys Rev Lett* 2018, *120*, 207801.

[5] L. Leibler, *Macromolecules* 1980, *13*, 1602.

[6] P. J. Flory, *Principles of Polymer Chemistry*, Cornell University Press, 1953.

[7] J. Brandrup, E. H. Immergut, E. A. Grulke, A. Abe, D. R. Bloch, *Polymer Handbook*, Wiley New York, 1999.

[8] M. Rubinstein, R. H. Colby, *Polymer Physics*, Oxford University Press New York, 2003.

[9] S. Nakano, M. Fujimoto, H. Hara, N. Sugimoto, *Nucleic Acids Res* 1999, *27*, 2957.

[10] J. N. Zadeh, C. D. Steenberg, J. S. Bois, B. R. Wolfe, M. B. Pierce, A. R. Khan, R. M. Dirks, N. A. Pierce, *J Comput Chem* 2011, *32*, 170.

[11] B. Jacrot, *Rep Prog Phys* 1976, *39*, 911.

[12] H. Chen, J. Zhang, W. Yu, Y. Cao, Z. Cao, Y. Tan, *Angewandte Chemie Int Ed* 2021, DOI 10.1002/anie.202105112.

[13] T. M. FitzSimons, F. Oentoro, T. V. Shanbhag, E. V. Anslyn, A. M. Rosales, *Macromolecules* 2020, *53*, 3738.

[14] D. E. Fullenkamp, L. He, D. G. Barrett, W. R. Burghardt, P. B. Messersmith, *Macromolecules* 2013, *46*, 1167.

[15] B. Marco-Dufort, R. Iten, M. W. Tibbitt, *J Am Chem Soc* 2020, *142*, 15371.